Cumhuriyet Sci. J., 46(3) (2025) 658-667
DOI: https://doi.org/10.17776/csj.1738296

Cumhuriyet Science Journal

| csj.cumhuriyet.edu.tr | Founded: 2002 ISSN: 2587-2680 e-ISSN: 2587-246X Publisher: Sivas Cumhuriyet University

Neutron Induced Fission Cross Section Calculation for Tungsten, Tantalum, Bismuth and Lead Nuclei Using Cem03.03 And TALYS

Murat Dağ [1,a,*]

[1] *Vocational School of Health Services, Kırşehir Ahi Evran University, Kırşehir, Türkiye*

**Corresponding author*

Research Article

History
Received: 09/07/2025
Accepted: 15/09/2025

ABSTRACT

Nuclear reaction data serve as indispensable input across a broad range of nuclear physics, including the improvement of theoretical models of nuclear interactions, nuclear structure studies, reactor design, nuclear transmutation, and radiation shielding. In particular, accurate neutron-induced fission cross section data over a wide range of neutron energies are essential not only for deepening our understanding of the fission process but also for developing a new generation of nuclear reactors that reduce the challenges associated with nuclear waste storage. However, in cases where experimental measurements for a specific nuclear reaction have not been performed or when obtaining such data is impracticable due to experimental challenges, computational simulations become critically important for determining the reaction cross sections. This work focused on neutron-induced fission cross sections of tungsten, tantalum, bismuth, and lead nuclei due to their primary use in accelerator-driven systems (ADS) as spallation targets and structural materials. Neutron-induced fission cross sections for the aforementioned nuclei have been calculated using CEM03.03, the latest version of the Cascade-Exciton Model, and TALYS 2.0, which integrates three level density models, Constant Temperature Model (CTM), The Back-Shifted Fermi Gas Model (BSFGM), and the Generalized Superfluid Model (GSM). These model based calculations are compared both with each other and with experimental data from the literature and evaluated data libraries. This study aims to (i) guide future theoretical and experimental efforts in nuclear fission research; (ii) highlight energy ranges where additional experimental measurements are needed; and (iii) identify areas in computational modelling that require improvement, to help validate model accuracy.

Keywords: Neutron-induced fission, ADS, Sub-actinide, CEM03.03, TALYS.

[a] *muratdag@ahievran.edu.tr* *https://orcid.org/0000-0002-0503-6067*

Introduction

As global energy demand continues to rise, nuclear energy holds a significant option in meeting this demand only if its certain challenges, such as management and disposal of radioactive waste safely and effectively, is properly managed [1,2]. One promising strategy to this issue is Partitioning and Transmutation (P&T) technologies, which helps the substantial reduction of radiotoxicity (harmful radiation emissions) and thermal load (heat generated by decay) by transforming long-lived radionuclides into short-lived or stable isotopes.

Accelerator-Driven Systems (ADS), which integrate P&T methods, have emerged as encouraging nuclear technologies what is both capable of both generating clean energy and effectively incinerating nuclear waste [3-6]. Consequently, ADS offers a practical and promising framework for the mitigation of radioactive waste. In this context, fission cross section measurement is important to guide the optimization in ADS, particularly neutron-induced fission cross sections are critically significant for ADS applications, given that sub-actinide isotopes such as tungsten, tantalum, bismuth, and lead serve important roles as spallation targets and structural materials. However, when empirical cross-section data are unavailable or experimentally impractical to obtain, computational modeling becomes indispensable for providing reliable theoretical predictions.

In this study, neutron-induced fission cross sections for the aforementioned isotopes across a wide range of neutron energy range were computed using CEM03.03 and TALYS with three level density models. The results of the model-based calculations were systematically compared with available experimental data from established nuclear data libraries. Through this comparative analysis, the study seek to evaluate the accuracy and reliability of these nuclear reaction models compared to experimental data, and identify areas requiring further computational improvement, and highlight the crucial need for more extensive experimental measurements.

Method

TALYS is a widely recognized nuclear reaction simulation code, renowned for its reliable predictive capabilities across a comprehensive range of nuclear reaction scenarios. Developed to handle nuclear reactions involving diverse projectiles such as neutrons, photons, protons, deuterons, tritons, helium-3 nuclei, and alpha particles, TALYS operates effectively for projectile energies up to 200 MeV and targets with mass numbers of 12 and above. TALYS offers a user-friendly computational environment that enables researchers to readily adjust input parameters, thereby modifying simulations to align with their targeted research purposes. Continuous updates and

enhancements ensure TALYS remains at the forefront of nuclear reaction modeling, supported by extensive experimental datasets. This ongoing refinement process significantly improves the accuracy and reliability of its predictions [7-8].

In TALYS, multiple level density models are implemented, ranging from phenomenological expressions to those derived from microscopic models. In this study it has been focused using three level density models in TALYS: the Constant Temperature Model (CTM) [9], the Back-Shifted Fermi Gas Model (BSFGM) [10-12], and the Generalized Superfluid Model (GSM) [13-15].

The level density, ρ(Ex, J,Π), represents the number of nuclear levels per MeV around an excitation energy Ex for given spin J and parity Π. The total level density sums over all spins and parities

$$\rho_{\text{tot}}(E_x) = \sum_{J,\Pi} \rho(E_x, J, \Pi) \quad (1)$$

Fermi Gas Model (FGM) is one of the well-known analytical level density expression, based on assumption that the single-particle states constructing the excited levels of the nucleus are equally spaced and that collective levels are unavailable. For a two-fermion system—i.e., differentiating between excited neutrons and protons—the total Fermi gas state density is written as:

$$\omega_F^{tot}(E_x) = \frac{\sqrt{\pi}\exp[2\sqrt{aU}]}{12\,a^{1/4}U^{5/4}}; \quad U = E_x - \Delta, \quad (2)$$

where the energy shift Δ is an empirical parameter equal to, or closely related in some models to, the pairing energy added to simulate the known odd–even effects in nuclei. Summing the Fermi gas level density over all spins and parities yields for the total Fermi gas level density as

$$\rho_F^{tot}(E_x) = \frac{\omega_F^{tot}(E_x)}{\sqrt{2\pi}\sigma} \quad (3)$$

which can be expressed such as

$$\rho_F^{tot}(E_x) = \frac{\omega_F^{tot}(E_x)}{\sqrt{2\pi}\sigma} \quad (4)$$

The equation above shows that ρ_F^{tot} is determined by three parameters: the energy shift parameter Δ , the spin cut-off parameter σ, and the level density parameter a. The first two terms Δ and σ are energy-dependent paremeters. The level density parameter a as stated in Eq. 5 is the coefficient that governs how rapidly the number of available nuclear levels grows with excitation energy in the Fermi-gas expression. Early approaches [9,11,16] treat the level density parameter as a parameter independent of energy. Later, Ignatyuk et. al. [13,17] introduced an energy dependence into a to phenomenologically fold in shell-correction effects—large at low excitation and vanishing at high excitation.

$$a = a(E_x) = \tilde{a}\left(1 + \delta W \frac{1-\exp[\gamma U]}{U}\right) \quad (5)$$

Here, the asymptotic level density ã in Eq. 5 is given as

$$\tilde{a} = \alpha A + \beta A^{2/3} \quad (6)$$

ã represents the asymptotic level-density value when shell effects are absent; in other words, ã generally equals $a(E_x)$ as the excitation energy E_x approaches infinity. However, if the shell-correction energy δW is zero, then ã is equal to $a(E_x)$ for all excitation energies. The damping parameter γ determines how quickly $a(E_x)$ approaches ã. Lastly, δW quantifies the shell-correction energy: its magnitude determines how much $a(E_x)$ deviates from ã at low excitation energies, while its sign indicates whether $a(E_x)$ increases or decreases with E_x.

In the CTM, as introduced by Gilbert and Cameron, excitation energy range is divided into a low energy part up to a matching energy EM and a high energy part above EM. The model assumes the nucleus behaves like a system at constant nuclear temperature for low excitation energies, but for higher energies, the Fermi gas model given by Eq. 3 is more suitable. The BSFGM, on the other hand, uses the Fermi gas expression stated in Eq. 3, and treats the pairing energy as an adjustable parameters. In this model, pairing shift in the energy shift is an adjustable parameter to fit experimental data per nucleus, while in the CTM uses no adjustable pairing shift parameters by default. The GSM takes account of superconductive pairing correlation as outlined in the Bardeen-Cooper-Schrieffer theory. In its phenomenological form, as developed by Ignatyuk et. al. [14,17] , the model transitions from a superfluid behaviour at low energy, where pairing correlations dominate the level density, to a high energy region described by the FGM. Unlike the CTM, which distinguishes between a low energy and a high energy region, the distinction of energy region of the GSM emerges naturally from the theory.

The Cascade-Exciton Model (CEM), on the other hand, is a sophisticated computational framework utilized to simulate nuclear reactions initiated by nucleons, pions, and photons. Developed approximately thirty years ago by researchers Gudima, Mashnik, and Toneev at the Laboratory of Theoretical Physics, Joint Institute for Nuclear Research (JINR), in Dubna, USSR, CEM systematically describes nuclear reactions through three interconnected phases: intranuclear cascade, pre-equilibrium processes, and subsequent evaporation or fission of the excited compound nucleus [18-20].

During the initial intranuclear cascade phase, an incoming projectile particle, such as a nucleon or photon, collides with nucleons inside the target nucleus. This interaction generates secondary particles, which may either continue participating in additional intranuclear interactions or become absorbed within the nuclear medium. At the conclusion of this stage, the residual nucleus remains highly excited, prompting it to transition into the pre-equilibrium phase. During the pre-equilibrium stage, the excited nucleus continues to undergo complex internal processes as energy redistribution occurs among nuclear constituents. Finally, in the evaporation or fission stage, the compound nucleus reaches equilibrium and either emits particles (such as neutrons, protons, or alpha particles) or fragments via fission.

In CEM, after the cascade stage of a reaction, but before reaching statistical equilibrium at a defined time teq, we get

$$\eta_{eq} \simeq \sqrt{2gE} \quad (7)$$

The parameter g is related to the level density parameter of single particle states, $a=\pi^2 g/6$, and E is excitation energy of the nucleus . At the preequilibrium stage, the level density parameter a is defined in CEM as its own approximation [21] in the form proposed initially by Ignatyuk et. al. [13] , following by Iljinov et. al. [22] as

$$a(Z,N,E^*) = \tilde{a}(A)\left\{1+\delta W_{gs}(Z,N)\frac{f(E^*-\Delta)}{E^*-\Delta}\right\} \quad (8)$$

$$\tilde{a}(A) = \alpha A + \beta A^{\frac{2}{3}} B_s \quad (9)$$

Eq. 9 is the asymptotic Fermi-gas value of the level density parameter at high energies. Bs defines as the ratio of the surface ares of the nucleus to the surface area of a sphere of the same volume (equal to ≈1 for the ground state). The total excitation energy of the nucleus E^* is related to the thermal energy and defines by E^*-E_R-Δ, where E_R and Δ are the rotational and pairing energies, respectively. In CEM, the shell correction by Möller et. al. [23] and the pairing energy shifts from Möller, Nix, and Kratz [24] are used.

CEM03.03 is the latest version of the model, offering enhanced predictive accuracy and computational efficiency relative to earlier iterations. This latest version leverages advanced Monte Carlo simulation techniques and significant improvements in modeling pre-equilibrium dynamics and evaporation processes. The intranuclear cascade component of CEM03.03 employs a modernized adaptation of the traditional Dubna cascade model, which has been substantially refined in recent years at the Los Alamos National Laboratory (LANL). A particularly feature of CEM03.03 is the integration of the latest version of the Modified Exciton Model (MEM), which meticulously captures the complexities inherent in the pre-equilibrium interactions. Following this, the evaporation and fission processes are simulated by incorporating the improved Generalized Evaporation Model (GEM2) developed by Furihata. These significant enhancements emphasize a shift toward more physics-based modeling, reducing reliance on empirical approximations and thereby increasing predictive reliability and efficiency, especially for intermediate-mass nuclei.

By integrating extensive experimental datasets and refining its computational techniques, CEM03.03 delivers precise predictions at high incident neutron energies. This makes the model broadly applicable across areas, including nuclear physics and nuclear astrophysics. Crucially, CEM03.03 excels in predicting secondary particle production—an essential capability for applications in nuclear medicine, radiation safety assessments, and shielding design. Furthermore, it significantly contributes to advancing fundamental theoretical insights into nuclear structure and dynamics.

Neutron-induced cross sections of the sub-actinide isotopes 181Ta, 182W, 183W, 184W, 186W, 204Pb, 206Pb, 207Pb, 208Pb, and 209Bi are significant for ADS application given that they serve important roles as spallation targets and structural materials. Hence, in this study, these isotopes were chosen as target to assess the performance of different nuclear models: CEM03.03 and TALYS with three different level density models (CTM, BSFGM, GSM). For each target, neutron induced fission cross sections were computed using each model's default parameter settings over neutron energies up to 1000 MeV. The calculated fission cross sections were compared with experimental data extracted from EXFOR database. Since the incident energies of neutron in the experimental data do not always match the simulated energy points, interpolation techniques were used to estimate model predictions at the exact experimental energies in order to evaluate each model performance. This approach provided an efficient way of comparison while minimizing required computional demand. To quantify model performance, reduced chi-squared (χ^2/N) were calculated to assess each model.

Results

In this study, cross sections of ^{181}Ta(n,f), ^{182}W(n,f), ^{183}W(n,f), ^{184}W(n,f), ^{186}W(n,f), ^{204}Pb(n,f), ^{206}Pb(n,f), ^{207}Pb(n,f), ^{208}Pb(n,f), and ^{209}Bi(n,f) reactions were calculated for three level density models using TALYS 2.0 code in incident neutron energy range of 10-1000MeV. The calculated results and available experimental data are presented in Figure 1-10 along with evaluated data libraries (experiments from EXFOR data libraries, ENDF/B-VIII, TENDL-2019, JENDL).

As seen in Figure 1, CEM03.03 closely matches the experimental data up to 200 MeV. CTM and BSFGM yield nearly identical results, but decline more rapidly than CEM03.03 at high energies. GSM significantly overpredicts the cross sections throughout the entire energy range. As shown in Figure 2, CEM03.03 exhibits the closest agreement with both experimental measurements and evaluated library data, whereas CTM and BSFGM moderately underpredict the cross sections. GSM significantly overpredicts the fission cross section across the entire energy region.

As depicted in Figure 3, CEM03.03 accurately reproduces experimental data points. CTM and BSFGM slightly overpredict the magnitude of cross sections at low energies, but at high energies underpredict the cross sections, while GSM markedly overestimates the cross sections by several factors. As seen in Figure 4, CEM03.03 provides the most reliable agreement with the experimental data compared to other models. CTM and BSFGM capture the general shape but exhibit overprediction up to 150 MeV and underprediction at energies above 150 MeV, both showing a declining trend at higher energies. GSM systematically and significantly overpredicts the cross sections across the entire energy range.

As illustrated in Figure 5, CEM03.03 demonstrates consistent agreement with experimental data throughout the entire energy range. CTM captures the overall trend but moderately underpredicts at high energies. BSFGM slightly overestimates cross sections at low energies, whereas GSM significantly overpredicts across all energies. As seen in Figure 6, CEM03.03 predictions show reliable agreement with the experimental data. CTM, BSFGM, and GSM capture the general shape but systematically overpredict the cross sections, particularly at higher energies.

As shown in Figure 7, CEM03.03 aligns closely with experimental measurements up to 200 MeV and maintains good consistency at higher energies. CTM and BSFGM moderately predict the data but have a tendency toward systematic overestimation, while GSM consistently and substantially overpredicts the fission cross sections. As seen in

Figure 8, CEM03.03 closely follows the experimental data, accurately capturing the overall trend and maintaining excellent agreement across the full energy range. CTM provides moderately good agreement up to approximately 200 MeV. BSFGM systematically overpredicts at low energies and slightly underpredicts the data at higher energies. GSM consistently overpredicts the cross sections, especially at energies below 150 MeV.

As seen in Figure 9, CEM03.03 and CTM exhibit the best agreement with the experimental data up to 200 MeV, with CEM03.03 continuing to maintain good agreement over the entire energy range. BSFGM and GSM systematically overpredict the cross sections, particularly at low and intermediate energies. As shown in Figure 10, CEM03.03 consistently demonstrates the closest agreement with experimental data across the entire energy range. CTM maintains moderately good agreement up to about 200 MeV but shows some deviations at higher energies. BSFGM and GSM both systematically overpredict the fission cross sections, with GSM exhibiting more pronounced deviations.

For ^{181}Ta, CEM03.03 outperforms TALYS models by about 90%, with CTM and BSFGM showing moderate agreement but roughly 30–50% less accurate predictions. In the case of ^{182}W, CEM03.03 again leads with approximately 85% better fit compared to GSM, while CTM and BSFGM perform well at low energies but lose accuracy at higher energies. For ^{183}W, CEM03.03 provides the most reliable results, roughly 80% more accurate than the consistent overprediction by GSM; CTM and BSFGM diverge increasingly beyond 200 MeV. Similarly, ^{184}W's fission cross sections are best described by CEM03.03, surpassing GSM by more than 85%, while CTM and BSFGM accuracy decreases by 35–45% at higher energies. With ^{186}W, CEM03.03 maintains strong estimation across all energies, outperforming TALYS level density models by over 80%, as GSM significantly overestimates the cross sections. For ^{204}Pb, CEM03.03 exceeds GSM by over 90%, with CTM and BSFGM models fitting well at low energies but losing up to 50% at higher energies. In ^{206}Pb, CEM03.03 remains about 75–85% more accurate than GSM; CTM and BSFGM lose reliability as energy increases. For ^{207}Pb, CEM03.03 is approximately 80% closer to experimental data than GSM, with CTM and BSFGM accuracy decreasing by around 40% over the extended energy range. In the case of ^{208}Pb, CEM03.03 outperforms GSM by more than 85%, while CTM and BSFGM decline in accuracy by up to 45% at higher energies. Finally, for ^{209}Bi, CEM03.03 shows nearly 90% better agreement compared to GSM, with CTM and BSFGM models performing reasonably below 200 MeV but degrading notably at higher neutron energies.

Neutron-induced fission cross sections of sub-actinide isotopes such as ^{181}Ta, ^{182}W, ^{183}W, ^{184}W, ^{186}W, ^{204}Pb, ^{206}Pb, ^{207}Pb, ^{208}Pb, and ^{209}Bi play a crucial role in Accelerator-Driven Systems (ADS), where these nuclei serve as both spallation targets and structural components. In this study, we evaluated the predictive capabilities of the CEM03.03 model alongside TALYS with three level density models—CTM, BSFGM, and GSM—over neutron energies extending up to 1000 MeV. Our comparison, based on reduced chi-squared values interpolated to match experimental energies, shows that CEM03.03 consistently aligns more closely with measured data across both low (0–200 MeV) and broad (0–1000 MeV) energy ranges. TALYS models using CTM and BSFGM generally perform adequately at lower energies but tend to diverge more noticeably as energy increases. On the other hand, the GSM model tends to systematically overestimate fission cross sections throughout the full energy spectrum, with the discrepancy growing at higher energies. These observations suggest that while CTM and BSFGM effectively capture nuclear structure effects at lower energies, all three models' parameterizations such as level density parameter, fission barries height, fission barrier width etc. may require refinement to maintain accuracy, especially at high energies. Meanwhile, the GSM's consistent overprediction points to inherent challenges within its current theoretical approach for these isotopes. In conclusion, CEM03.03 provides a reliable description of neutron induced fission across the studied energy range, underscoring its suitability for ADS nuclear data evaluations.

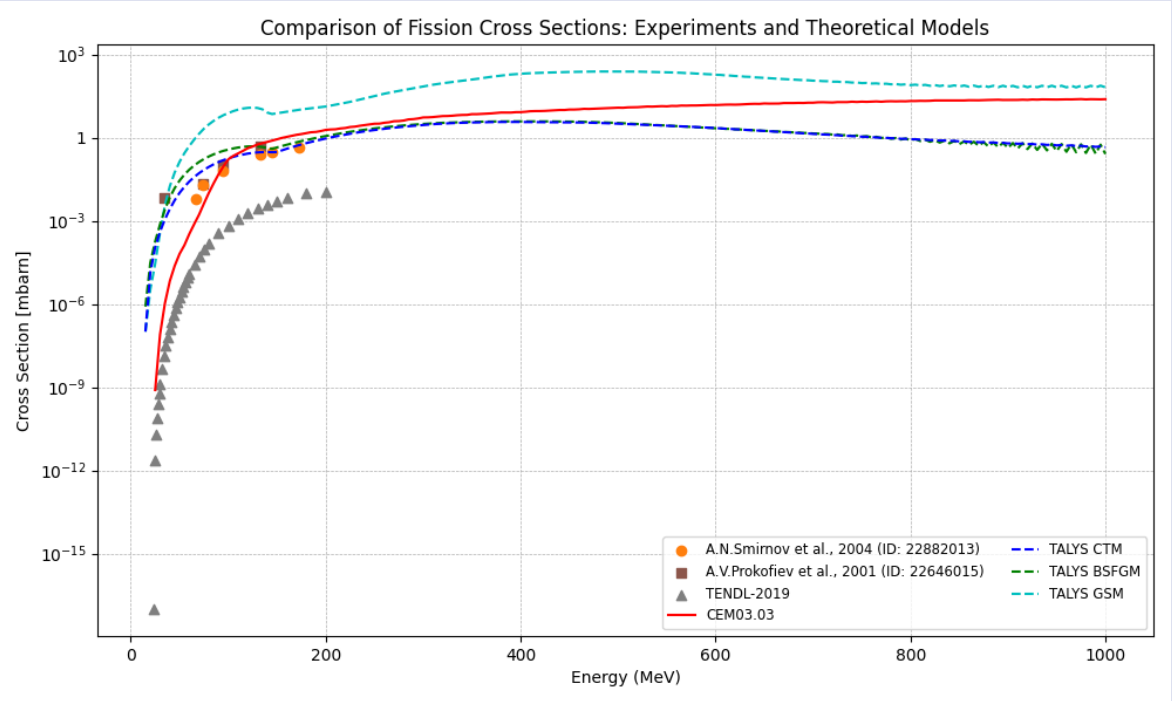

Figure 1. Neutron-induced fission cross sections of ^{181}Ta. The calculated cross sections were compared with available experimental data from EXFOR and evaluated data libraries.

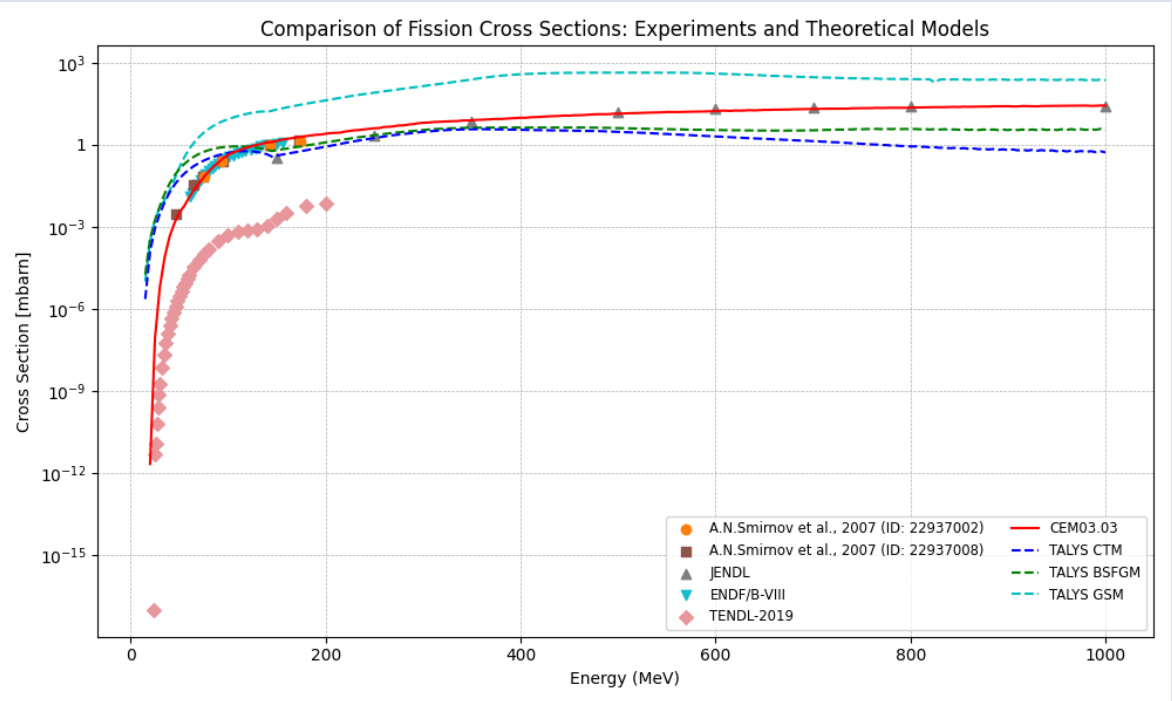

Figure 2. Neutron-induced fission cross sections of ^{182}W. The calculated cross sections were compared with available experimental data from EXFOR and evaluated data libraries.

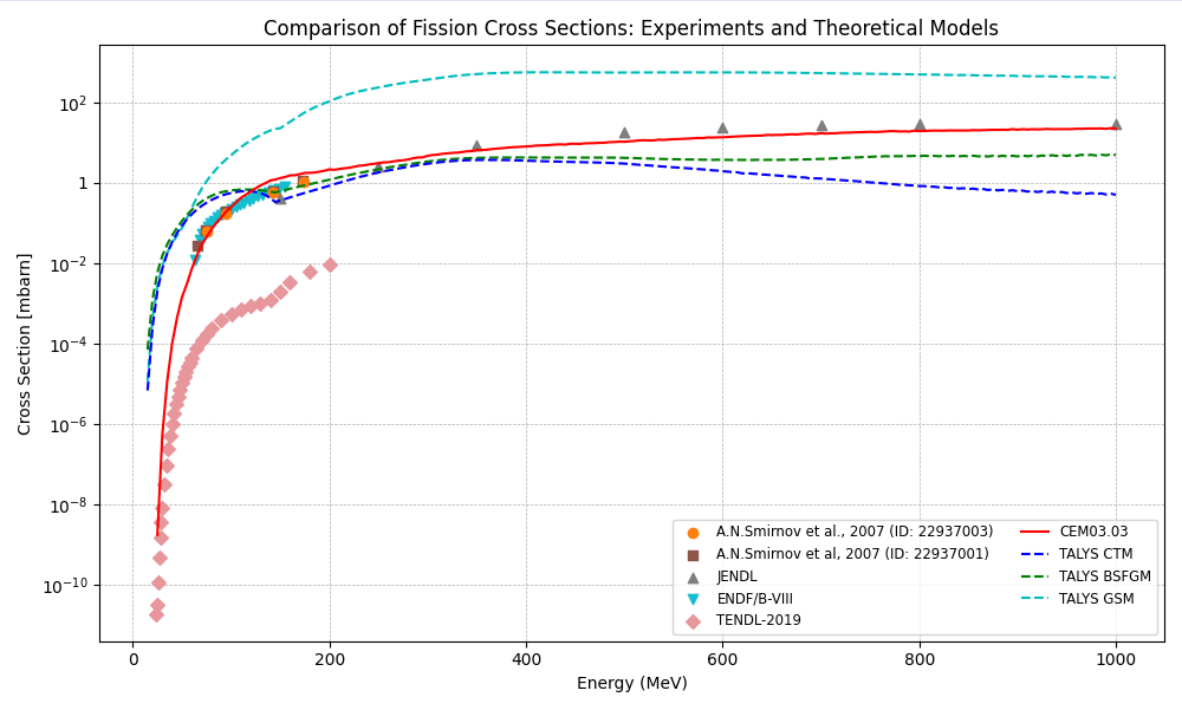

Figure 3. Neutron-induced fission cross sections of ^{183}W. The calculated cross sections were compared with available experimental data from EXFOR and evaluated data libraries.

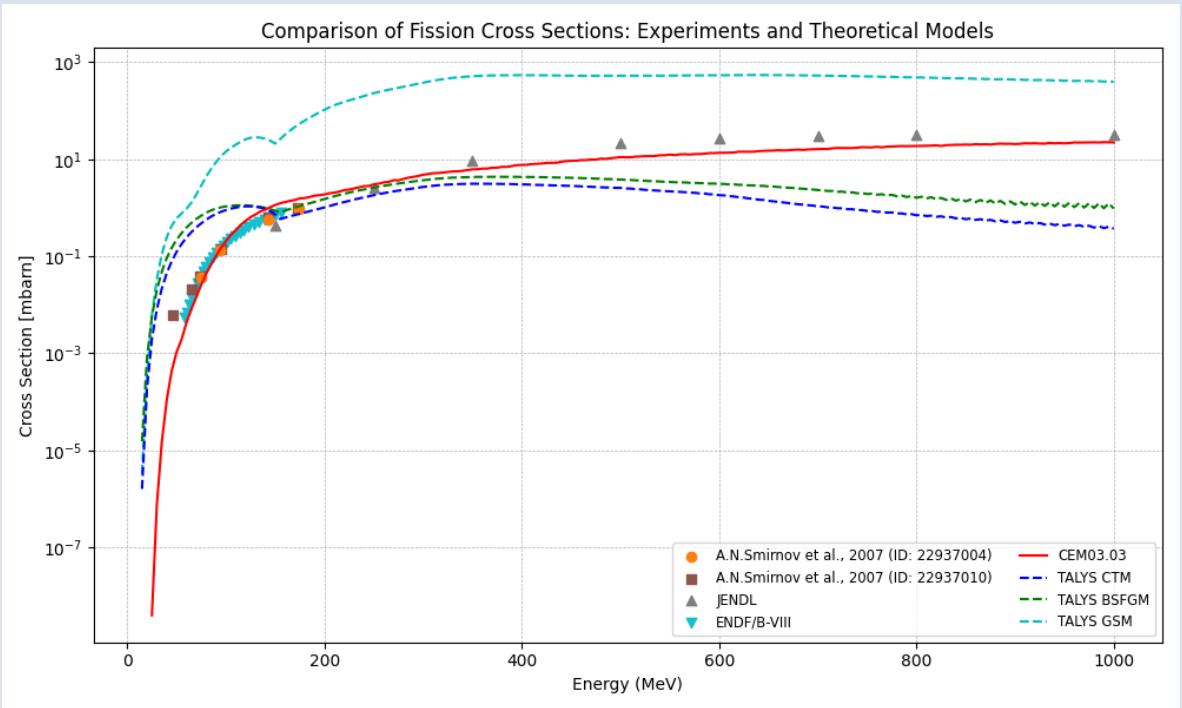

Figure 4. Neutron-induced fission cross sections of ^{184}W. The calculated cross sections were compared with available experimental data from EXFOR and evaluated data libraries.

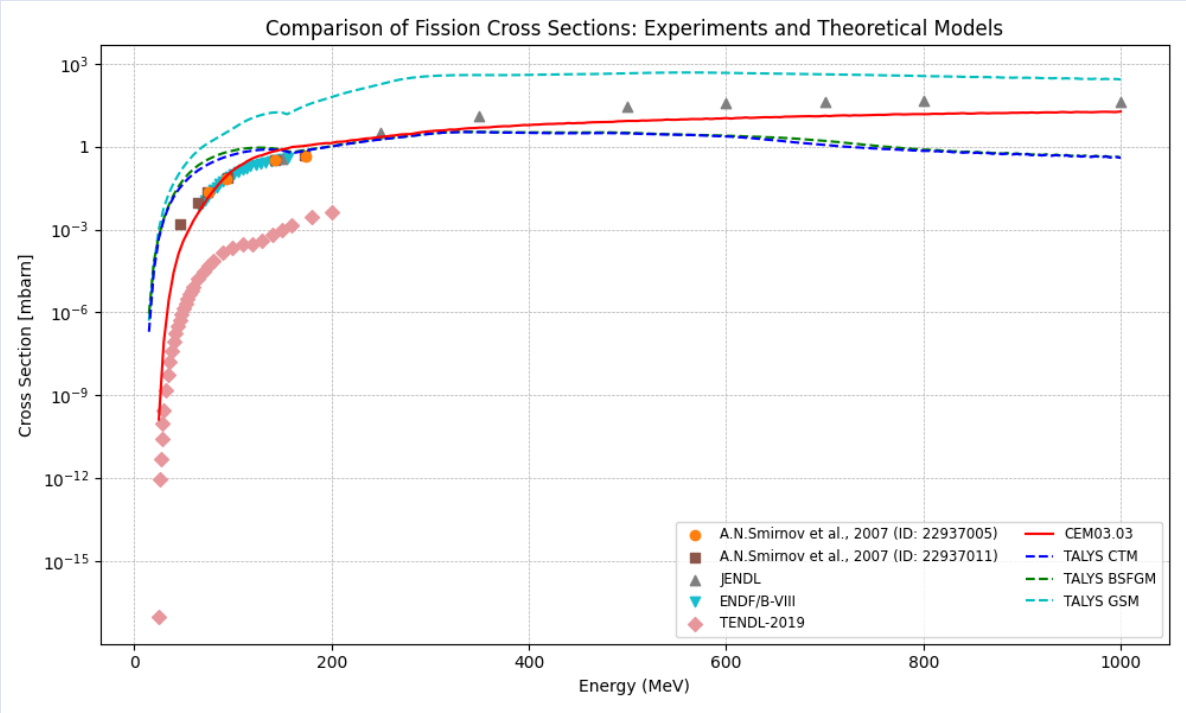

Figure 5. Neutron-induced fission cross sections of ^{186}W. The calculated cross sections were compared with available experimental data from EXFOR and evaluated data libraries.

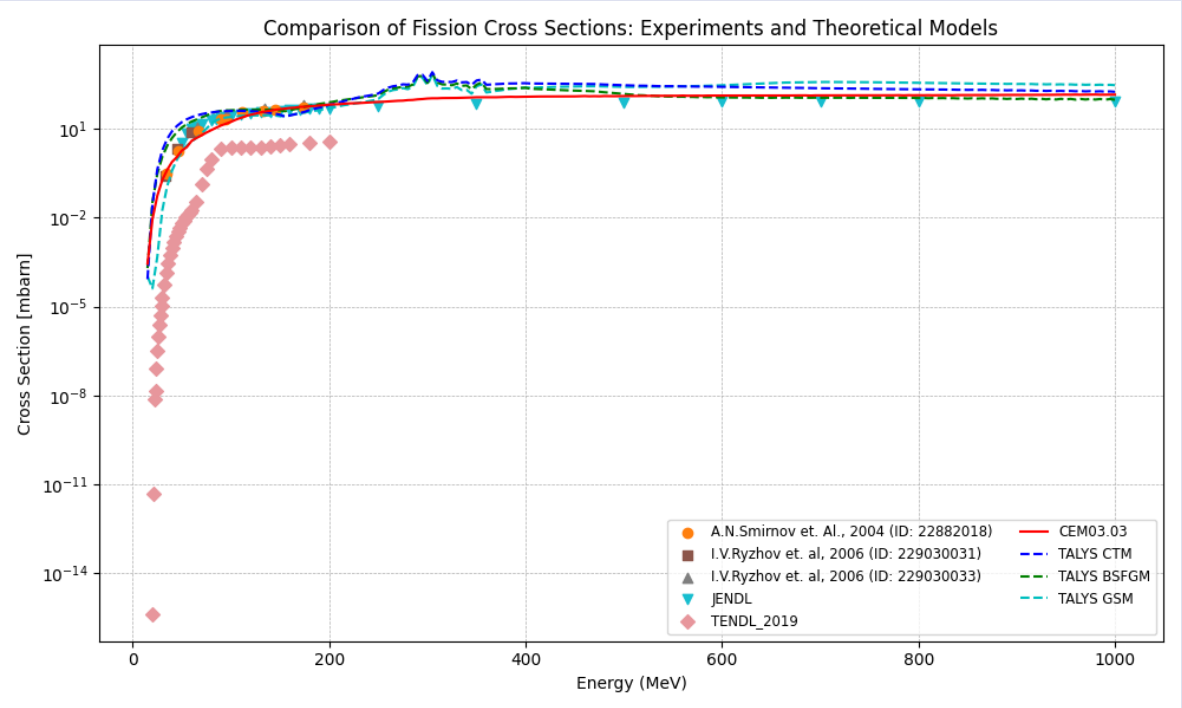

Figure 6. Neutron-induced fission cross sections of ^{204}Pb. The calculated cross sections were compared with available experimental data from EXFOR and evaluated data libraries.

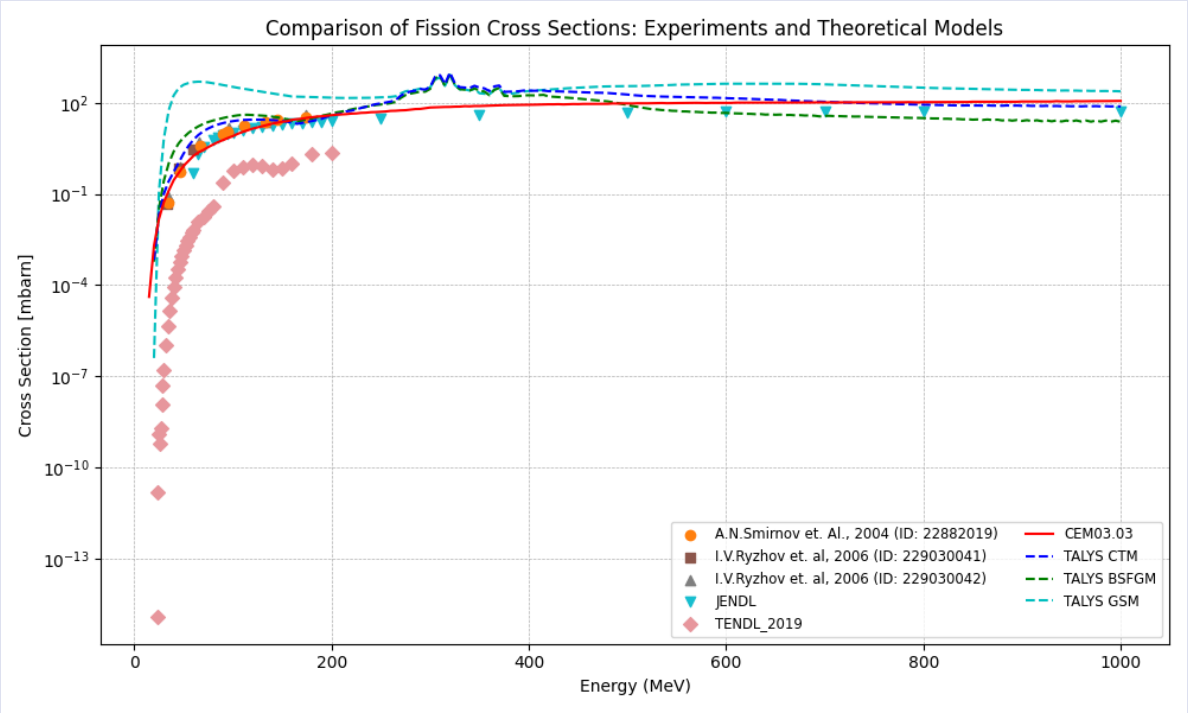

Figure 7. Neutron-induced fission cross sections of ^{206}Pb. The calculated cross sections were compared with available experimental data from EXFOR and evaluated data libraries.

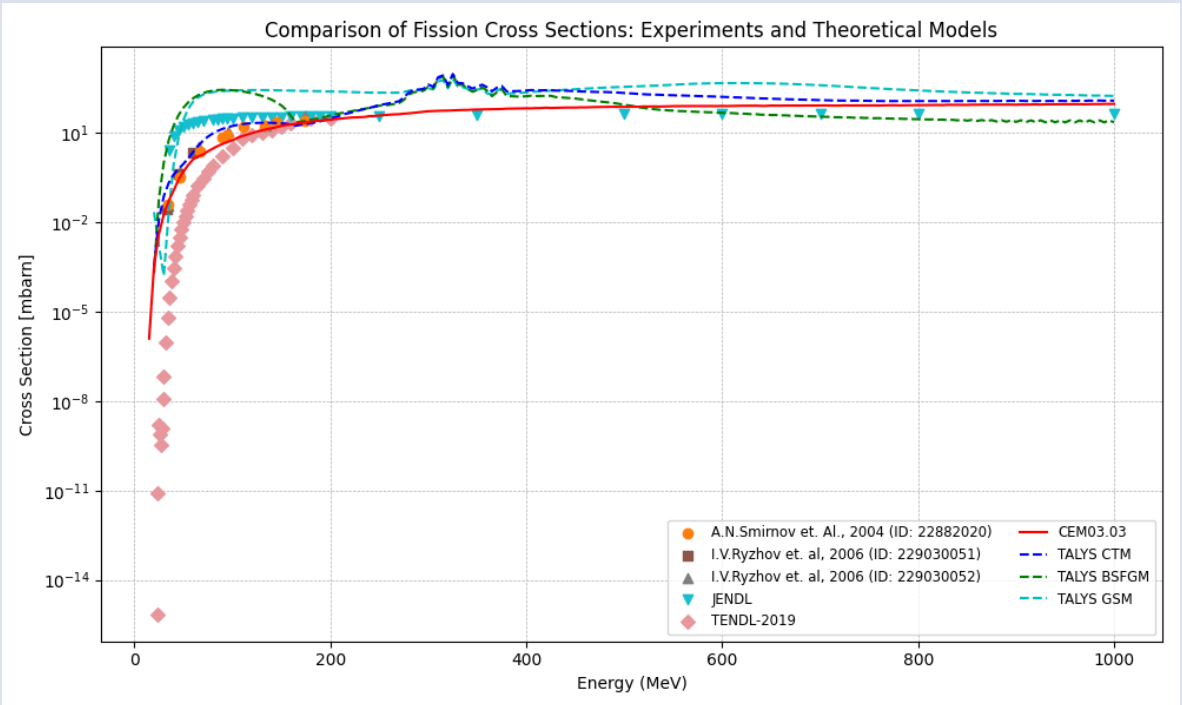

Figure 8. Neutron-induced fission cross sections of ^{207}Pb. The calculated cross sections were compared with available experimental data from EXFOR and evaluated data libraries.

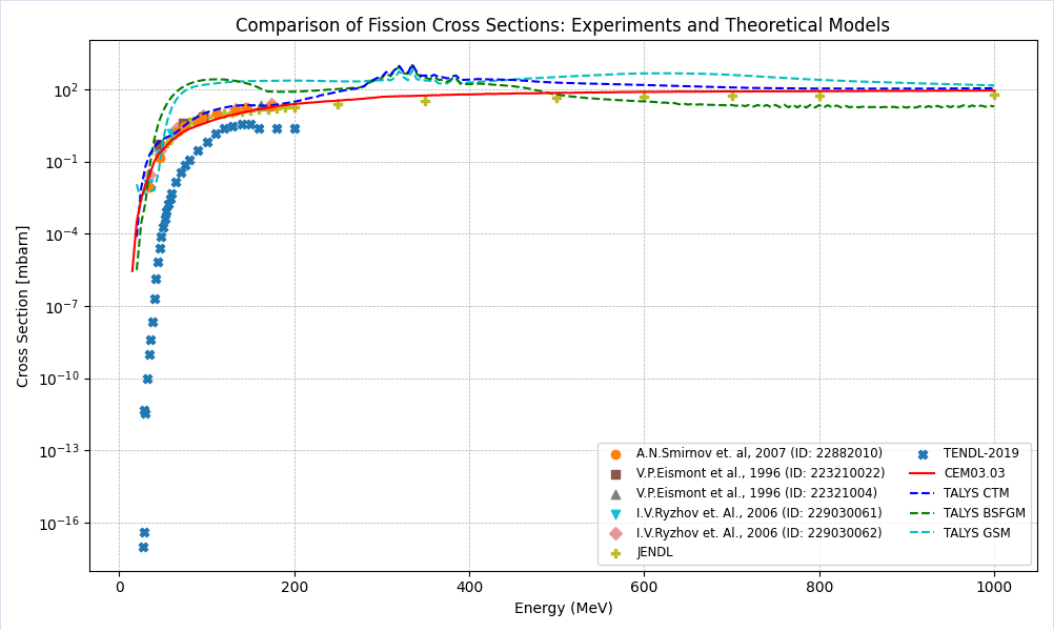

Figure 9. Neutron-induced fission cross sections of ^{208}Pb. The calculated cross sections were compared with available experimental data from EXFOR and evaluated data libraries.

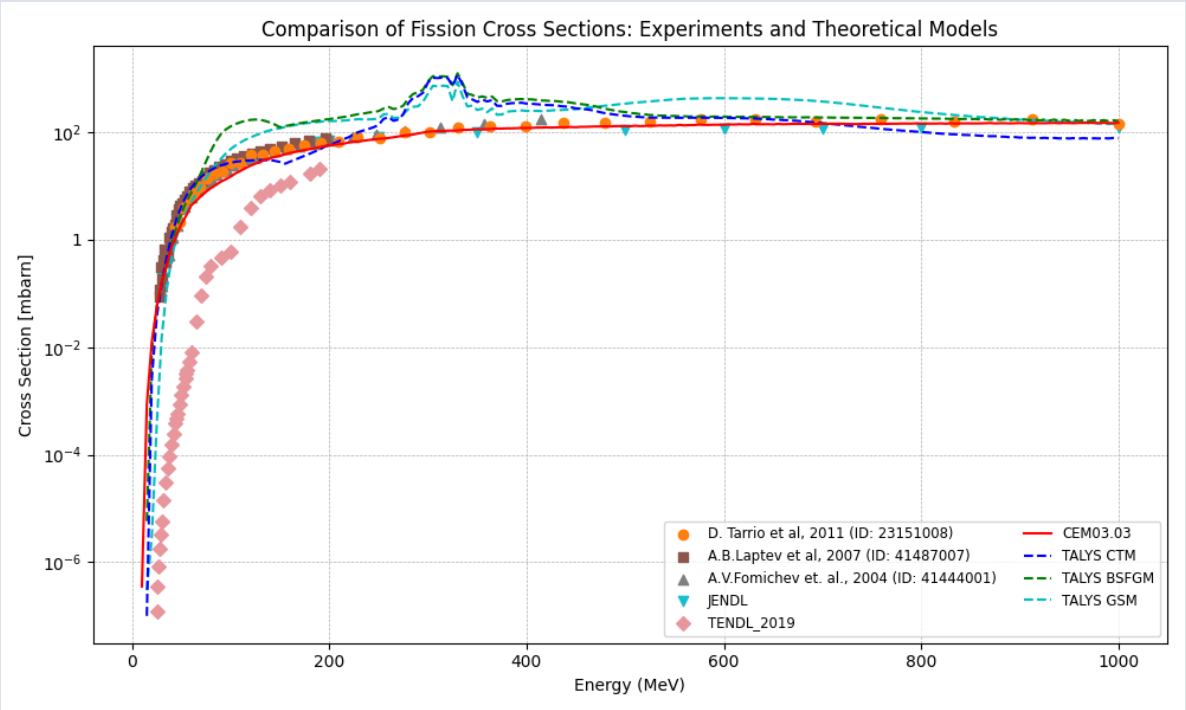

Figure 10. Neutron-induced fission cross sections of ^{209}Bi. The calculated cross sections were compared with available experimental data from EXFOR and evaluated data libraries.

Conflicts of interest

There are no conflicts of interest in this work.

References

[1] I.A.E. Agency, Climate Change and Nuclear Power 2020, *Climate Change and Nuclear Power*, 1 (2020).

[2] Mathew M.D., Nuclear Energy: A Pathway towards Mitigation of Global Warming, *Prog. Nucl. Energy*.

[3] Nuclear Energy Agency, Accelerator-Driven Systems (ADS) and Fast Reactors (FR) in Advanced Nuclear Fuel Cycles: A Comparative Study. Available at: https://www.oecd-nea.org/upload/docs/application/pdf/2019-12/nea3109-ads_fr.pdf. Retrieved July 28, 2025.

[4] Kumar V.V., Katovsky K., A Comprehensive Review of Developments of Accelerator Driven Subcritical Systems and Future Requirements, in: 2020 21st International Scientific Conference on Electric Power Engineering (EPE), Prague, (2020) 1-6.

[5] Luo R., Revankar S.T., Zhang D., Zhao F., Inherent Safety Characteristics of Lead Bismuth Eutectic-Cooled Accelerator Driven Subcritical Systems, *Front. Energy Res.*, 10 (2022).
[6] Maschek W., Granget G., Kondo M., Sugimoto M., Accelerator driven systems for transmutation: Fuel development, design and safety, *Prog. Nucl. Energy*, 50 (2008) 333-339.
[7] Koning A.J., Hilaire S., Goriely S., Global and local level density models, *Nucl. Phys. A*, 810 (2008) 13-76.
[8] Koning A.J., Hilaire S., Goriely S., TALYS-1.96/2.0 Simulation of Nuclear Reactions, 2021.
[9] Gilbert A., Cameron A.G.W., A Composite Nuclear-Level Density Formula With Shell Corrections, *Can. J. Phys.*, 43 (1965) 1446-1496.
[10] Demetriou P., Goriely S., Microscopic nuclear level densities for practical applications, *Nucl. Phys. A*, 695 (2001) 95-108.
[11] Dilg W., Schantl W., Vonach H., Uhl M., Level density parameters for the back-shifted fermi gas model in the mass range 40 < A < 250, *Nucl. Phys. A*, 217 (1973) 269-298.
[12] Grossjean M.K., Feldmeier H., Level density of a Fermi gas with pairing interactions, *Nucl. Phys. A*, 444 (1985) 113-132.
[13] Ignatyuk A.V., Smirenkin G.N., Tishin A.S., Phenomenological description of energy dependence of the level density parameter, *Yad. Fiz.*, 21 (1975) 485-495.
[14] Ignatyuk A.V., Istekov K.K., Smirenkin G.N., Role of collective effects in the systematics of nuclear level densities, *Sov. J. Nucl. Phys.*, 29 (1979).
[15] Ignatyuk A.V., Weil J.L., Raman S., Kahane S., Density of discrete levels in 116Sn, *Phys. Rev. C*, 47 (1993) 1504-1510.
[16] Baba H., A shell-model nuclear level density, *Nucl. Phys. A*, 159 (1970) 625-634.
[17] Ignatyuk A.V., Weil J.L., Raman S., Kahane S., Density of discrete levels in 116Sn, *Phys. Rev. C*, 47 (1993) 1504-1510.
[18] Mashnik S.G., Sierk A.J., CEM03.03 User Manual and the MCNP6 Code Package, Los Alamos National Laboratory, (n.d.).
[19] Mashnik S.G., Sierk A.J., Gudima K.K., Baznat M.I., The MCNP6 Event Generator CEM03.02: Lessons Learned from the Intercomparison, Los Alamos National Laboratory, (2010).
[20] Mashnik S.G., Sierk A.J., Recent developments of the cascade-exciton model of nuclear reactions, *J. Nucl. Sci. Technol.*, 39 (2002) 720-722.
[21] Sierk A.J., Mashnik S.G., Modeling Fission in the Cascade-Exciton Model, Los Alamos National Laboratory, (1998).
[22] Iljinov A.S., Mebel M.V., Bianchi N., De Sanctis E., Guaraldo C., Lucherini V., Muccifora V., Polli E., Reolon A.R., Rossi P., Phenomenological statistical analysis of level densities, decay widths and lifetimes of excited nuclei, *Nucl. Phys. A*, 543 (1992) 517-557.
[23] Möller P., Nix J.R., Myers W.D., Swiatecki W.J., Nuclear Ground-State Masses and Deformations, *At. Data Nucl. Data Tables*, 59 (1995) 185-381.
[24] Möller P., Nix J.R., Myers W.D., Swiatecki W.J., Nuclear Ground-State Masses and Deformations, *At. Data Nucl. Data Tables*, 59 (1995) 185-381.Möller P., Nix J.R., Kratz K.L., Nuclear properties for astrophysical and radioactive-ion-beam applications, *At. Data Nucl. Data Tables*, 66 (1997) 131-343.